Available online at www.sciencedirect.com
SCIENCE DIRECT
Journal of Colloid and Interface Science 295 (2006) 551–561
JOURNAL OF Colloid and Interface Science
www.elsevier.com/locate/jcis

Transient electroosmotic flow induced by AC electric field in micro-channel with patchwise surface heterogeneities

Win-Jet Luo *

Department of Electronic Engineering, Far East College, Tainan, Taiwan

Received 4 May 2005; accepted 24 September 2005

Available online 19 October 2005

Abstract

This paper investigates two-dimensional, time-dependent electroosmotic flow driven by an AC electric field via patchwise surface heterogeneities distributed along the micro-channel walls. The time-dependent flow fields through the micro-channel are simulated for various patchwise heterogeneous surface patterns using the backwards-Euler time stepping numerical method. Different heterogeneous surface patterns are found to create significantly different electrokinetic transport phenomena. The transient behavior characteristics of the generated electroosmotic flow are then discussed in terms of the influence of the patchwise surface heterogeneities, the direction of the applied AC electric field, and the velocity of the bulk flow. It is shown that the presence of oppositely charged surface heterogeneities on the micro-channel walls results in the formation of localized flow circulations within the bulk flow. These circulation regions grow and decay periodically in phase with the applied periodic AC electric field intensity. The location and rotational direction of the induced circulations are determined by the directions of the bulk flow velocity and the applied electric field.

Keywords: Electroosmotic flow; Patchwise surface heterogeneity

1. Introduction

The term "electroosmotic flow" refers to the fluid flow induced by an externally applied electric field along a charged surface. Electroosmotic flow is a fundamental electrokinetic phenomenon exploited in a diverse range of practical applications. Recent innovations in microfluidic systems designed for biological and chemical "laboratories on a chip" have prompted intensive research efforts to enhance the efficiency and throughput of these systems. In developing microfluidic devices, it is frequently necessary to devise the means to drive fluids from one part of the device to another, to control the fluid motion, to enhance mixing, or to separate fluids. Electroosmosis provides an attractive means of manipulating liquids in such devices. A significant advantage of the electroosmosis phenomenon is that the voltages applied at the device reservoirs can be used not only to control the bulk fluidic transport, but also to drive the separation of the different components of a sample in accordance with their differing electrophoretic mobilities.

In the main, previous studies have focused on DC electroosmotic flows in straight conduits with uniform potentials along the conduit walls [1–4]. However, time periodic electroosmotic flows and AC electroosmosis have also attracted considerable academic attention. Investigating the transient phenomena of electroosmotic flow is important in enhancing the operation of biochips and improving their separation efficiency. Soderman and Jonsson [5] and Santiago [6] presented theoretical frameworks describing the behavior of the transient electroosmotic flow under the Debye–Huckel linear approximation. Oddy et al. [7] presented an analytical flow field model for an axially applied AC electric field in an infinitely wide microchannel, and demonstrated experimentally a series of schemes for enhanced species mixing in microfluidic devices. Dutta and Beskok [8] developed an analytic model for an applied sinusoidal electric field using a non-linear Poisson–Boltzmann double layer distribution. Studer et al. [9] presented a fabrication technique which enabled the realization of microfluidic devices incorporating electrodes with smaller feature sizes. The

* Fax: +886 6 597 7570.
E-mail address: wjluo@cfd.es.ncku.edu.tw.

0021-9797/$ – see front matter
doi:10.1016/j.jcis.2005.09.052

authors demonstrated that the resulting devices were capable of supporting such novel functionalities as the injection, mixing, and separation of bio-molecules by means of AC electrokinetic pumping. Green et al. [10] applied a nonuniform AC electric field to an electrolyte using coplanar microelectrodes to generate a steady fluid flow. The flow was driven at the surface of the electrodes such that it moved in a plane normal to the electrode surface. The impedance of the double layer on the electrodes and the potential drop across the double layer have been studied both experimentally and theoretically using linear analysis. Luo [11] and Luo et al. [12] used numerical simulations based on the stream function and vorticity formulations to investigate the transient electroosmotic flow induced by DC and AC electric fields in a curved micro-tube. The transient secondary flow evolutions provided clear evidence of the growth and decay of vortices in the transverse section.

Recently, Ajdari [13] studied complex electroosmotic flows induced by nonuniform, time-independent, and time-dependent potentials along the conduit walls. Nonuniform potentials can be obtained by coating the walls of the conduit with different materials or by using different buffer solutions. Both spatial and temporal control of the potential can be achieved by imposing an electric field perpendicular to the solid–liquid interface. These normal electric fields can be imposed by electrodes embedded beneath the solid–liquid interface and insulated electrically from the liquid. Alternatively, when the surface of the solid conduit is photosensitive, the surface charge can be modified with light. Oddy et al. [7] developed an electrokinetic process to enhance the stirring of micro- and nano-liter volume solutions for microfluidic bioanalytical applications. Their study presented a preliminary description of the electrokinetic instability and exploited this flow phenomenon to design and fabricate two micro-mixing devices capable of rapidly stirring two fluid streams. Qian and Bau [14] performed a theoretical investigation of two-dimensional, time-independent, and time-dependent electroosmotic flows driven by a uniform electric field in a conduit with nonuniform potential distributions along the walls. Their results demonstrated that the time-wise periodic alternations of the potentials induced a chaotic advection effect. Strook et al. [15] presented the measurement of electroosmotic flows in micro-channels with two different surface charge patterns and reported that diverse fluid behaviors were induced in the flows. Erickson and Li [16] employed three-dimensional numerical simulations to study the effects of surface electrokinetic heterogeneities on the electroosmotic flow induced by a uniform electric field and then exploited these effects to enhance the mixing efficiency of a T-shaped micro-mixer. The numerical results confirmed that surface heterogeneities can enhance species mixing. Furthermore, it was shown that the greatest improvements were obtained when the potential of the heterogeneous surface was of the opposite sign to that of the homogeneous surface. Biddiss et al. [17] developed experimental visualizations to investigate the effects of surface charge patterning on the species mixing and presented an optimized electrokinetic micro-mixer applicable to the low Reynolds number regime. Chang and Yang [18] used a numerical method to simulate the mixing mechanisms of

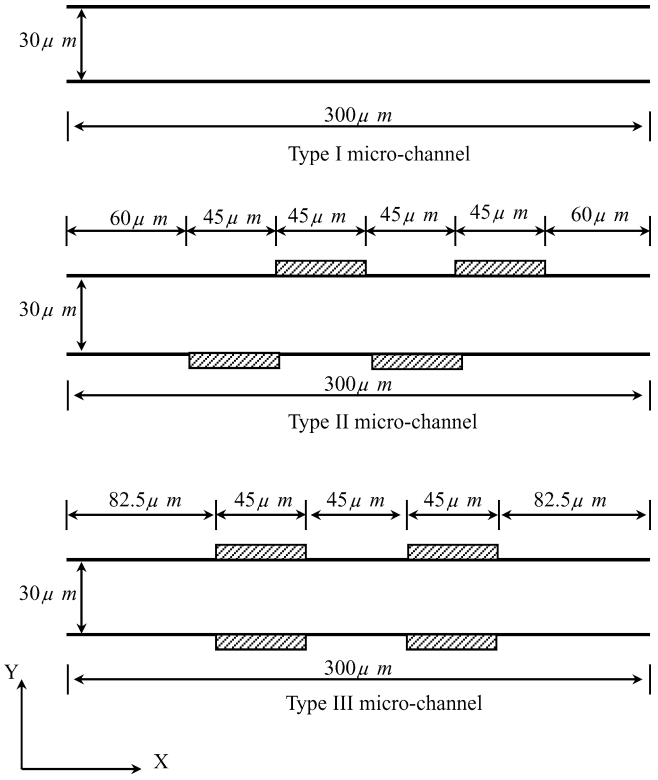

Fig. 1. Geometry of current micro-channels with height of 30 μm and width of 0.3 mm. Note heterogeneous regions are crosshatched.

electroosmotic flow induced by a DC electric field in a micro-channel with oppositely charged surface heterogeneities. The results showed that local flow circulations promote species mixing in micro-channels. Lee et al. [19] investigated the characteristics of electroosmotic flow in a cylindrical micro-channel with nonuniform zeta potential distribution with a numerical method. They demonstrated that using either heterogeneous patterns of zeta potential or a combination of a heterogeneous zeta potential distribution and an applied pressure difference over the channel can generate local flow circulations and hence provide effective means to improve the mixing between different solutions in micro-channels.

Electrokinetic flow is widely used to conduct species transport in a number of biological and chemical analysis systems. These analysis systems, which are designed to conduct immunoassays, DNA hybridization, and general cell molecule interaction applications, must be capable of achieving a rapid mixing effect. Furthermore, applications of these systems typically involve the mixing of reagents with relatively low diffusion coefficients. Rapid homogeneous mixing becomes increasingly important when the time scale of the mixing activity is larger than, or comparable to, the chemical reaction time scale. In the present study, micro-channels with patchwise surface heterogeneities are designed to enhance the mixing efficiency by means of a periodic electroosmotic flow induced by a sinusoidal externally applied electric field. As shown in Fig. 1, the present study considers three different micro-channels, namely one micro-channel with an entirely homogeneous surface, and two micro-channels with different surface heterogeneity dis-

tributions. In all cases, the flow is driven through the micro-channel under the influence of a sinusoidal AC electric field applied by two electrodes installed at either end of the channel. A numerical method is adopted to simulate the transient phenomena of the electroosmotic flow. Using the backwards-Euler time stepping method, numerical solutions are obtained for the stream-function and vorticity transport equations, which govern the velocity fields of the electroosmotic flow. The transient behavior characteristics of the generated electroosmotic flow are then discussed in terms of the influence of the patchwise surface heterogeneities, the direction of the applied AC electric field, and the velocity of the bulk flow. The current investigations of transient behavior provide detailed insights into the characteristics of electroosmotic flow and are consequently of fundamental importance in understanding and enhancing biochip operations. It is anticipated that the application of oppositely charged surface heterogeneities and an AC electric field to the flow in the microfluidic system will reduce not only the mixing channel length, but also the retention time required to obtain a homogeneous solution.

2. Formulation

This study considers a micro-channel of height 30 μm and length 300 μm. The channel is filled with an incompressible Newtonian electrolyte of uniform dielectric constant, ε, and viscosity, μ. It is assumed that this fluid is in a stationary state initially. Since the characteristic height of the micro-channel is in the order of magnitude of 10 μm, the interaction of the fluid and the wall is significant and must be considered in the theoretical model. A review of the related literature identifies a suitable theoretical model for the micro-channel. This model has been widely exploited by previous researchers and is described by the Poisson–Boltzmann equation, the Laplace equation, and the Navier–Stokes equation comprising the body force terms from the Guoy–Chapman model. The distribution of the electrical double layer potential is described by the Poisson–Boltzmann equation, and the induced electroosmotic flow in the micro-channel is governed by the momentum equations.

2.1. Double-layer field

When the liquid in the micro-channel contacts the solid wall, an interfacial charge is established which causes the free ions in the liquid to rearrange so as to form a thin region with non-zero net charge density. This region is commonly referred to as the electrical double layer (EDL). According to electrostatics theory, the electric potential distribution in the EDL region is governed by the Poisson–Boltzmann equation [20], which is expressed as:

$$\frac{\partial^2\psi}{\partial x^2}+\frac{\partial^2\psi}{\partial y^2}=\frac{2n_0ze}{\varepsilon}\sinh(ze\psi/k_bT),$$

where ε is the dielectric constant of the fluid medium, z is the valence, e is the charge of an electron, n_0 is the bulk electrolyte concentration, k_b is the Boltzmann constant, and T is the temperature. Non-dimensional quantities (denoted by asterisks) can be defined as:

$$x^*=\frac{x}{A},\quad y^*=\frac{y}{A},\quad \psi^*=\frac{ze\psi}{k_bT}.$$

The dimensionless non-linear Poisson–Boltzmann distribution equation is then given by:

$$\frac{\partial^2\psi}{\partial x^2}+\frac{\partial^2\psi}{\partial y^2}=\kappa^2\sinh(\psi), \tag{1}$$

where ψ is the non-dimensional EDL potential, $\kappa=A\times K$ is the non-dimensional EDL thickness, $K=(2n_0z^2e^2/\varepsilon\varepsilon_0k_bT)^{1/2}$ is the Debye–Huckel parameter, and A is the height of the micro-channel. (Note that the asterisks are deliberately omitted in these equations.)

2.2. Electroosmotic flow field

When an external electric field is applied, the liquid flow induced by electroosmosis is governed by the momentum equations [8,21], i.e.,

$$\rho\frac{\partial V}{\partial t}+\rho(V\cdot\nabla)V=-\nabla P+F+\mu\nabla^2V. \tag{2}$$

If the gravity effect is neglected, the body force, F, occurs only as a result of the action of the applied electric field on the free ions within the EDL. This body force induces a bulk fluid motion generally referred to as electroosmotic flow.

The following non-dimensional quantities (denoted by asterisks) can be introduced: non-dimensional velocity: $u^*=u/(\upsilon/A)$ or $v^*=v/(\upsilon/A)$, non-dimensional time: $t^*=t/(A^2/\upsilon)$, non-dimensional pressure: $p^*=(p-p_{\text{ref}})/(\rho\upsilon^2/A^2)$, and non-dimensional angular velocity: $\Lambda^*=\Lambda/(\upsilon/A^2)$, where υ is the kinetic viscosity of the electrolyte, t is time, and Λ is the angular velocity of the applied electric field, i.e. $\Lambda=2\pi f$. Hence, the momentum equations of Eq. (2) can be rewritten as:

$$\frac{\partial u}{\partial x}+\frac{\partial v}{\partial y}=0, \tag{3a}$$

$$\frac{\partial u}{\partial t}+u\frac{\partial u}{\partial x}+v\frac{\partial u}{\partial y}+\frac{\partial p}{\partial x}-\frac{\partial^2u}{\partial x^2}-\frac{\partial^2u}{\partial y^2}-G_x\cdot\sinh\psi\left(\frac{\partial\psi}{\partial x}+\frac{\partial\phi}{\partial x}\right)=0, \tag{3b}$$

$$\frac{\partial v}{\partial t}+u\frac{\partial v}{\partial x}+v\frac{\partial v}{\partial y}+\frac{\partial p}{\partial y}-\frac{\partial^2v}{\partial x^2}-\frac{\partial^2v}{\partial y^2}-G_x\cdot\sinh\psi\left(\frac{\partial\psi}{\partial y}+\frac{\partial\phi}{\partial y}\right)=0, \tag{3c}$$

where $Gx=2n_0k_bT/(\rho v^2/A^2)$ and ϕ is the applied electric potential. Reynolds number is defined as: uA/υ; hence, according to the definition of non-dimensional velocity quantity, the Reynolds number in the study equals to one as shown in Eqs. (3b) and (3c). The stream function, S, is defined as:

$$u=\frac{\partial S}{\partial y},\quad v=-\frac{\partial S}{\partial x}. \tag{4}$$

The continuity Eq. (3a) can then be satisfied by substituting Eq. (4) into Eq. (3a). The pressure terms, i.e. P, can be eliminated from Eqs. (3b) and (3c) by cross-differentiation, i.e., by taking the curl of the two-dimensional momentum equations. The vorticity-transport equation can be derived as:

$$\frac{\partial \Omega}{\partial t} - \frac{\partial S}{\partial y}\frac{\partial \Omega}{\partial x} - \frac{\partial S}{\partial x}\frac{\partial \Omega}{\partial y} - \left[\frac{\partial^2 \Omega}{\partial x^2} + \frac{\partial^2 \Omega}{\partial y^2}\right] - G_x \cdot \cosh\psi \frac{\partial \phi}{\partial x}\frac{\partial \psi}{\partial y} = 0. \tag{5}$$

Furthermore, the vorticity, Ω, is given by:

$$\Omega + \frac{\partial^2 S}{\partial x^2} + \frac{\partial^2 S}{\partial y^2} = 0. \tag{6}$$

The zeta potential distribution in the EDL can be obtained by solving Eq. (1), and the applied electric potential ϕ can be obtained by solving the Laplace equation. The transient electroosmotic flow under an applied electric field can be simulated by substituting of the calculated electric potential into Eq. (5) and solving the simplified equation set of Eqs. (5) and (6). By taking the cross-differentiation operation, the total number of dependent variables is reduced to just two, i.e. (S, Ω), and the body force terms from the Guoy–Chapman model in Eqs. (3b) and (3c) can be simplified. The boundary conditions of the zeta potential on the homogeneous surfaces of the micro-channel are -75 mV, and the corresponding dimensionless value is $\psi = -2.92$. The zeta potential on the heterogeneous surfaces is also 75 mV, and the corresponding dimensionless value is $\psi = 2.92$, as shown in Fig. 1. The boundary conditions at the walls, inlet, and outlet of the micro-channel are given by:

1. At the walls, with no slip conditions:

   $$\frac{\partial S}{\partial y} = 0, \quad \Omega + \frac{\partial^2 S}{\partial y^2} = 0, \quad \psi = -2.92$$

   on homogeneous surfaces and $\psi = 2.92$ on heterogeneous surfaces.
2. At the inlet and outlet:

   $$\frac{\partial^2 S}{\partial x^2} = 0, \quad \Omega + \frac{\partial^2 S}{\partial^2 y} + \frac{\partial^2 S}{\partial^2 x} = 0.$$

An implication in the above boundary conditions is that at the two ends of the micro-channel, the flow patterns are not going through any erupt changes. This condition can be ensured by applying constant zeta potentials near the end of the micro-channel, so that any changes in the electroosmotic flow field occur far away from the end boundaries. These boundary conditions may result in pressure gradient within the micro-channel. It should be noted the pressure difference between the two ends of the micro-channel is quite small in comparison with the body force in the micro-channel.

3. Numerical method

The present numerical method employs the backwards-Euler time stepping method to identify the evolutions of the flow when driven by an applied AC electric field. The computational domain is discretized into 151×201 non-equally spaced grid points in the X- and Y-directions. The calculated solutions are carefully proven to be independent of the computational grid points and the time step. The governing equations presented in Eqs. (5) and (6) are discretized by central differences of a second order to form a system of non-linear algebraic equations, i.e.,

$$H(Q, \Delta t) = 0, \tag{7}$$

where Q is the solution vector and Δt is the dimensionless marching time step.

The solution vector for various time-levels can be obtained via a sequence of iterations, i.e., $[Q^{(m)}(t)]$ defined by:

$$Q^{(0)}(0) \equiv \text{initial state}, \tag{8a}$$

$$H_Q(Q^{(m)}, \Delta t)\left[Q^{(m+1)}(t+\Delta t) - Q^{(m)}(t+\Delta t)\right] = -H(Q^{(m)}, \Delta t), \quad \text{where } m = 0, 1, 2, \ldots. \tag{8b}$$

In Eq. (8b), H_Q is the Jacobian matrix of Eq. (7), and t is the non-dimensional time.

A convergence criterion of

$$\left[Q^{(m+1)}(t+\Delta t) - Q^{(m)}(t+\Delta t)\right]^2 / Q(t)^2 < 10^{-16}$$

is used to identify the convergence of the iteration process. The convergence efficiency of the iteration is determined by the accuracy of the initial estimate. An appropriate initial estimate ensures that the iteration will converge efficiently. An effective means of obtaining good initial estimates is to employ a Taylor expansion of a calculated convergent solution with respect to the parameter Δt, i.e.

$$Q^{(0)}(t+\Delta t) = Q(t) + \Delta t\, Q_t(t). \tag{9}$$

Eq. (7) is used to obtain Q_t, which satisfies:

$$H_Q(Q, \Delta t)\, Q_t = -H_{\Delta t}(Q, \Delta t). \tag{10}$$

The method described in Eqs. (8)–(10) is known as the backwards-Euler time stepping method. Since this method employs a second order accuracy in time, it is necessary to provide two initial solutions at the beginning of the time stepping calculation. One of these solutions can be obtained from the initial state, while the other is obtained by using the same numerical method, but with a first order finite difference in time. Before the iteration algorithm is executed to obtain the convergence solution of the next time level, the predictor step in Eqs. (9) and (10) is applied to generate accurate estimates of the solution. Hence, the calculation algorithm is extremely effective and generally converges quadratically. A detailed description of this algorithm is reported in Yang [22].

4. Results and discussion

In this study, numerical simulations are performed of two-dimensional, time-dependent electroosmotic flows driven by a sinusoidal AC electric field through three different types of

Table 1
Typical values of the relevant quantities

A	Height of the micro-channel	30 μm
μ	Viscosity of fluid	0.90×10^{-3} N s/m^2
ρ	Density of fluid	10^3 kg/m^3
ζ	Concentration of ions	10^{-6} M
ε	Dielectric constant	78.3
ε_0	Permittivity of vacuum	8.854×10^{-12} F/m
e	Charge of an electron	1.6021×10^{-19} c
Z	Valence	1
n_0	Bulk electrolyte concentration	6.022×10^{20} m^{-3}
k_b	Boltzmann constant	1.38×10^{-23} J/K
T	Absolute temperature	298.16 K
ψ	Double layer potential	−75 mV
Λ^*	Non-dimensional frequency of the applied AC electric field	1

micro-channel, namely one micro-channel with an entirely homogeneous surface and two micro-channels with patchwise surface heterogeneities. In the latter micro-channels, the walls are characterized by patch regions charged with either a positive zeta potential, $\psi = |\psi_0|$, or with a negative zeta potential, $\psi = -|\psi_0|$. For clarity, the heterogeneous regions are cross-hatched in Fig. 1 and in thereinafter figures. The relevant micro-channel parameters are presented in Table 1.

4.1. Effects of surface heterogeneity on electrokinetic flow induced by DC electric field

In comparison with the flow phenomena induced by an AC electric field, Fig. 2 illustrates the flow conditions induced by a DC electric field which is generated by two electrodes installed at either end of the micro-channel. For the homogeneous case (Type I micro-channel) characterized by $\psi = |\psi_0|$, shown in Fig. 2a, the electroosmotic body force applied to the liquid continua within the double layer is equivalent at each point along the X-direction and results in a constant bulk liquid velocity at the edge of the double layer. For the case of two symmetrically positioned heterogeneous patches on the upper and lower micro-channel walls (Type III micro-channel), the phenomenon of constant bulk liquid velocity at the edge of the double layer also holds true for the heterogeneous surface with a negative zeta potential, i.e. $\psi = -|\psi_0|$, but the electroosmotic body force is now applied to a region with excess negative ions and hence acts in the opposite direction to that in the homogeneous regions. The interaction of these local flow fields with the bulk flow moving in the positive axial direction results in the formation of regional circulation zones which settle symmetrically adjacent to the heterogeneous surfaces, as shown in Fig. 2b. Fig. 2c illustrates the axial velocity distribution across the micro-channel cross section at locations near the interface of the homogeneous and heterogeneous regions. The liquid near the homogeneous surfaces is driven into motion in the positive axial direction. However, the liquid near the heterogeneous surfaces is driven into motion in the opposite axial direction. Due to flow rate conservation in the micro-channel, the axial velocity in the center of the heterogeneous regions is much greater than that in the center of the homogeneous regions. Along the X-axis, the axial velocity differentials between the flow in the wall regions and that in the central region of the micro-channel gradually increase and two reflection points are generated at locations close to the interface of the homogeneous and heterogeneous regions. The axial velocity differentials and reflection points prompt the formation of an anticlockwise rotational torque in the upper half of the heterogeneous regions and a clockwise rotational torque in the lower half of the heterogeneous regions. As a consequence, two vortices rotating symmetrically are formed in each heterogeneous region.

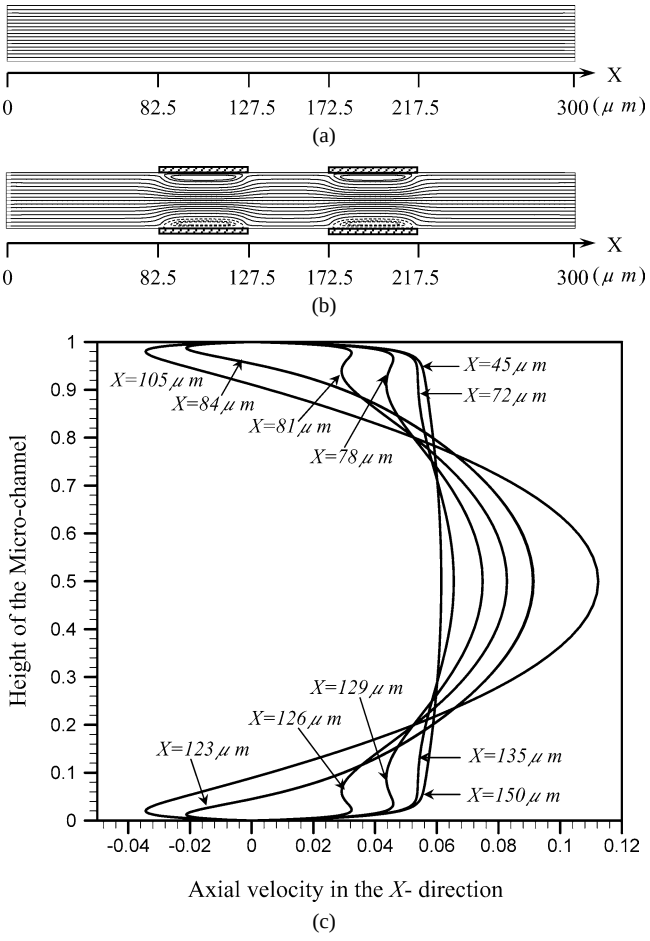

Fig. 2. (a) Flow conditions of electrokinetic flows induced by DC electric field in micro-channel with homogeneous surfaces. (b) Flow conditions of electrokinetic flows induced by DC electric field in micro-channel with symmetrical heterogeneous patches. (c) Axial velocity distributions of electrokinetic flows induced by DC electric field in micro-channel with symmetrical heterogeneous patches.

4.2. Electrokinetic flow induced by a sinusoidal electric field in Type II micro-channel

Using two electrodes installed at either end of the micro-channel, a sinusoidal electric field is applied to drive fluid through the Type II and Type III micro-channels. As shown in Fig. 3, the amplitude and frequency of the applied sinusoidal electric field are 450 V/cm and 1000 Hz, respectively. The dimensionless electric field along the X-direction is $\partial\phi/\partial x = 52.49\sin(2\pi t)$. Fig. 3 shows the evolution of the flow veloc-

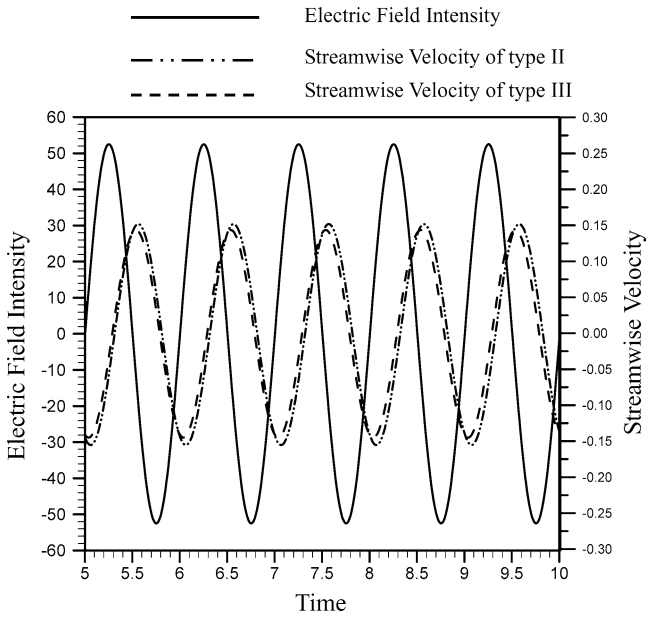

Fig. 3. Variation in applied sinusoidal electric field and streamwise velocities at half-height of micro-channel at $X = 30$ μm over time.

ity at the half-height of each of the two micro-channels at an axial location of $X = 30$ μm. The velocity evolutions provide an approximation of the variation of the streamwise bulk flow velocity over time. For the case of the Type II micro-channel, the variation of the streamwise velocity lags behind that of the electric field by a phase shift of approximately $\pi/2$ degrees. Meanwhile, in the Type III micro-channel, the streamwise velocity lags behind that of the electric field by a phase shift of approximately $\pi/2$ degrees. The direction of movement of the bulk flow in the Type II and Type III micro-channels determines the rotational direction of the induced circulations. The above phenomena are discussed in the following paragraphs.

Fig. 4 shows the flow evolutions in a micro-channel with a series of offset patches on the upper and lower walls (Type II micro-channel). At $t = 7$, no electrokinetic body force exists within the double layer, but the negative streamwise flow velocity of the micro-channel approaches its maximum value, as indicated in Fig. 3. Hence, the flow velocity in the entire micro-channel is in the negative X-direction, and the streamline contour has a stratified form. During the period from $t = 7$ to 7.5, the sinusoidal electric field applied to the micro-channel has a positive intensity, and the streamwise flow velocity along the micro-channel increases from its negative minimum value to its positive maximum value. Under these conditions, the fluid near the homogeneous surfaces is driven in the positive X-direction, while the fluid near the heterogeneous surfaces is driven in the negative X-direction. Hence, up-flows moving from the lower wall towards the upper wall and down-flows moving from the upper wall to the lower wall are formed at the boundaries of the homogeneous surfaces and the heterogeneous surfaces. The inertia force of the bulk flow in the negative direction causes these up-flows and down-flows to form circulations adjacent to the homogeneous surfaces. The circulations settled near the homogeneous regions of the lower wall rotate in the anticlockwise direction, while those near the homogeneous regions of the upper wall rotate in the clockwise direction. Due to the gradual increase over time in the intensity of the applied electric field and the corresponding reduction in the streamwise velocity of the bulk flow in the negative X-direction, the structures of these circulations gradually become more coherent, and grow in size and strength, as shown in Fig. 4a. Note that the circulations indicated with solid lines rotate in the anticlockwise direction, while those indicated with dashed lines rotate in the clockwise direction. The curved streamlines shown in Fig. 4a reveal the tortuous path through which the bulk flow must pass as a result of the offset, non-symmetric circulation regions. At $t = 7.25$, the intensity of the applied electric field reaches its positive maximum value, and the streamwise velocity in the micro-channel approaches zero. Therefore, the circulations occupy virtually the entire height of the micro-channel and obstruct the passage of flow in the axial direction. At this time, the intensity and size of the circulations approach their maximum values, and new sets of circulations rotating in an opposite direction to their neighboring circulations are induced in the heterogeneous regions. The alternating clockwise and anticlockwise rotating circulations arrange themselves sequentially along the axial direction. The size and intensity of these circulations are governed by the zeta potentials of the homogeneous and heterogeneous surfaces, the intensity of the applied electric field, the axial velocity of the bulk flow in the micro-channel, and the phase shift between the applied electric field and the velocity of the bulk flow. As time elapses, the intensity of the sinusoidal electric field applied to the micro-channel gradually decreases and the streamwise flow velocity at the half-height of the micro-channel at $X = 30$ μm increases from approximately zero to its positive maximum value. Meanwhile, the circulations adjacent to the homogeneous and heterogeneous surfaces gradually lose their strength and shrink in size. At $t = 7.5$, no electrokinetic body force exists within the double layer, but the streamwise velocity of the micro-channel approaches its positive maximum value. Hence, the flow velocity in the entire micro-channel becomes positive, and the streamline contour assumes a stratified form. During the second half of the cycle, i.e., from $t = 7.5$ to 8, the variation of the applied sinusoidal electric field intensity is the mirror image of the variation described from $t = 7$ to 7.5. Accordingly, the streamwise velocity of the micro-channel reverses from its positive maximum value to its positive–negative value. This causes the fluid flows within the double layer to reverse their respective directions of travel relative to the previous time period, i.e., the fluid near the homogeneous surfaces is driven in the negative X-direction, while the fluid near the heterogeneous surfaces is driven in the positive X-direction. As described above, the resulting up-flows, down-flows, and inertia forces of the bulk flow in the positive direction lead to the formation of local circulations adjacent to the homogeneous surfaces. The rotational directions of these newborn circulations are reversed with respect to the circulations observed in the previous time period, as shown in Fig. 4b. As before, the structures of the circulations gradually become more coherent over time, and grow in size and strength. Essentially, the evolution of the flow conditions during the cycle

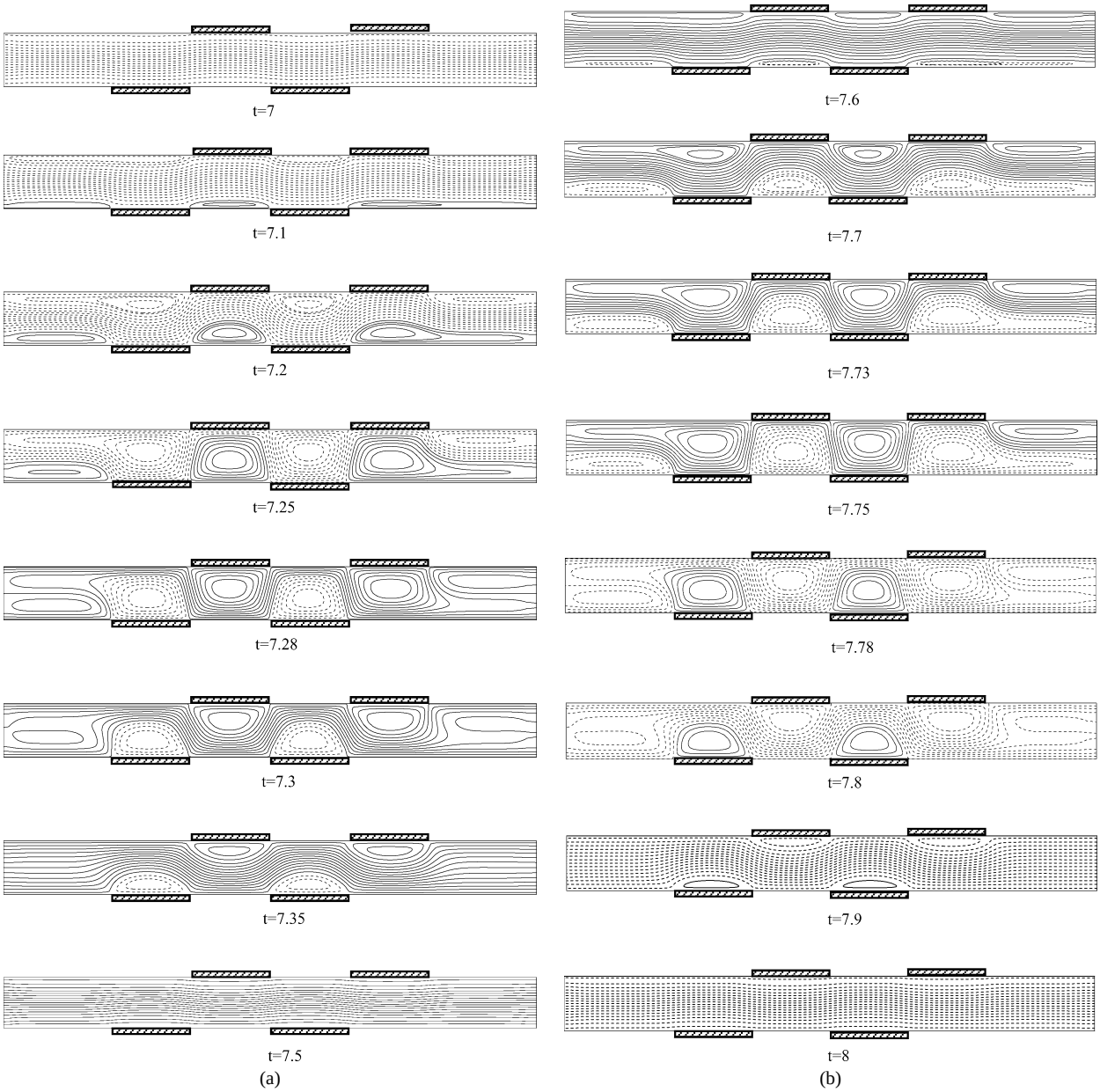

Fig. 4. (a) Flow evolutions in micro-channel with series of offset patches on upper and lower walls (Type II) during period $t = 7$–7.5. (b) Flow evolutions in micro-channel with series of offset patches on upper and lower walls (Type II) during period $t = 7.5$–8.

from $t = 7.5$ to 8 follows the same procedure as that described above $t = 7$–7.5. Clearly, however, the directions of the circulations and the bulk flow from $t = 7.5$ to 8 are reversed compared to those in the previous half-cycle. At time $t = 8$, the intensity of the applied electric field abruptly switches to the positive direction, and the streamwise velocity approaches its negative minimum value. The flow conditions at this time are identical to those observed at $t = 7$. Essentially, the evolution of the flow conditions during the cycle from $t = 8$ to 9 follows the same trend as that described above $t = 7$–8.

Fig. 5 indicates the axial velocity distributions along the Y-axis at $X = 45$ μm during a half period $t = 7$–7.5. At $t = 7$, the intensity of the applied electric field is zero, and the streamwise velocity approaches its negative minimum value. Consequently, no electrokinetic body force exists within the double layer, and the flow at the half-height of the micro-channel moves at its maximum velocity in the negative direction, as shown in Fig. 5. As the intensity of the applied AC electric field gradually increases over the period from $t = 7$ to 7.25 and then gradually decreases from $t = 7.25$ to 7.5, the fluid near the upper and lower walls accelerates in the positive direction ($t = 7$–7.25) and then decelerates in the positive direction ($t = 7.25$–7.5). The flow of fluid within the double layer drags the bulk fluid into motion in the positive direction only gradually since the momentum diffusion effects require a finite time to take effect. Therefore, the phase of the velocity at the half-height of the micro-channel lags behind that of the applied electric field by approximately $\pi/2$ degrees. The evolution of the velocity distribution along the Y-direction during next half period $t = 7.5$–8 follows a similar process to that described above

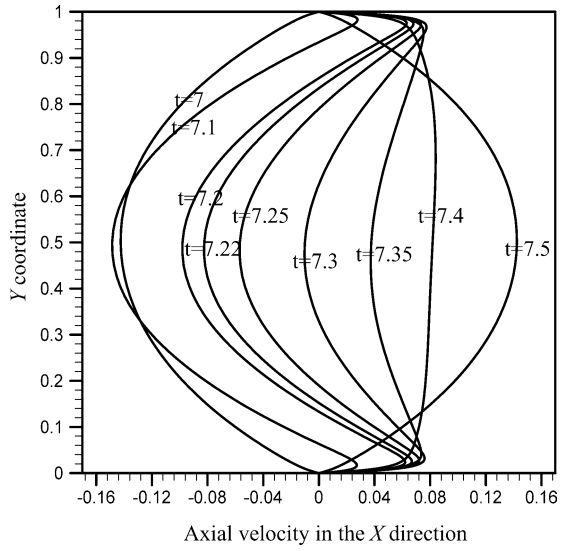

Fig. 5. Axial velocity distributions along Y-axis at $X = 45$ μm during period $t = 7$–7.5 in micro-channel with series of offset patches on upper and lower walls.

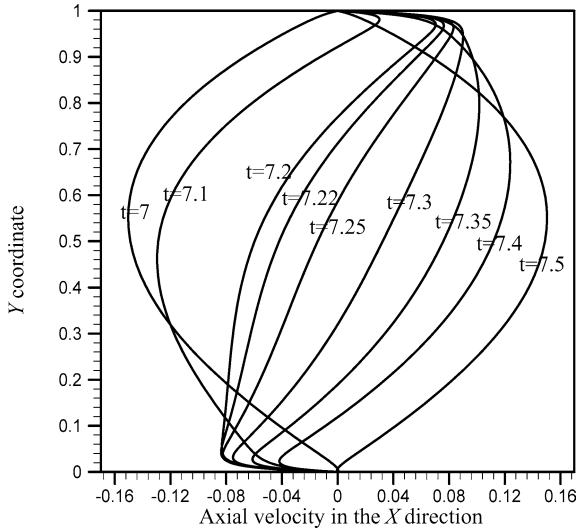

Fig. 6. Axial velocity distributions along Y-axis at $X = 82.5$ μm during period $t = 7$–7.5 in micro-channel with series of offset patches on upper and lower walls.

for $t = 7$–7.5. However, the direction of the fluid flow in the micro-channel is reversed.

Fig. 6 indicates the axial velocity distributions along the Y-axis at $X = 82.5$ μm during a half period $t = 7$–7.5. At $X = 82.5$ μm, the surface of the upper wall is homogeneous, while the surface of the lower wall is heterogeneous. During the period $t = 7$–7.5, the applied sinusoidal electric field has a positive intensity. In Fig. 6, as time elapses, the fluid within the double layer near the upper wall is gradually driven to move in the positive axial direction, while the fluid within the double layer near the lower wall is gradually driven to move in the opposite axial direction. Through momentum diffusion effects, the bulk flow is gradually dragged into motion from a negative velocity to a positive velocity in the axial direction. The velocity distribution along the Y-axis during the period $t = 7.5$–8 follows a similar evolution to that observed from $t = 7$ to 7.5. Clearly, however, the direction of flow in the micro-channel is reversed with respect to the previous half-cycle.

4.3. *Electrokinetic flow induced by a sinusoidal electric field in Type III micro-channel*

Fig. 7 illustrates the flow evolution in the micro-channel with two symmetrically positioned heterogeneous patches on the upper and lower micro-channel walls (Type III micro-channel). At $t = 7$, no electrokinetic body force exists within the double layer, but the negative flow velocity at the half-height of the micro-channel approaches its maximum value. Hence, the fluid velocity in the entire micro-channel is negative, and the streamline contour has a stratified form. During the period $t = 7$–7.5, the sinusoidal electric field applied to the micro-channel has a positive intensity, and the flow velocity at the half-height of the micro-channel increases from its negative minimum value to its positive maximum value. From $t = 7$ to 7.25, the fluid in the double layer near the homogeneous surfaces is driven in the positive axial direction, while the fluid in the double layer in the vicinity of the heterogeneous surfaces is driven in the negative axial direction. The interaction of the local flow fields with the bulk flow moving in the negative X-direction results in the formation of regional circulation zones which settle symmetrically adjacent to the homogeneous surfaces, as shown in Fig. 7a. The circulations adjacent to the lower wall rotate in the anticlockwise direction, while those adjacent to the upper wall rotate in the clockwise direction. Due to the gradual increase in the intensity of the applied electric field and the reduction in the velocity of the bulk flow in the negative X-direction, the structures of these circulations gradually become more coherent over time, and grow in size and strength. At $t = 7.25$, the intensity of the applied electric field reaches its maximum positive value, and the fluid velocity in the axial direction of the micro-channel is virtually zero. As a result, the intensity and size of the local circulations approach their maximum values, and new sets of circulations rotating in an opposite direction to their neighboring circulations are induced in the heterogeneous regions. The maximum size and intensity of the circulations depend on the zeta potentials of the homogeneous and heterogeneous surfaces, the intensity of the applied electric field, the velocity of the bulk flow, and the phase shift between the applied electric field and the bulk flow velocity. As time elapses, the intensity of the sinusoidal electric field applied to the micro-channel gradually decreases and the streamwise velocity of the micro-channel increases from zero to its positive maximum value. Meanwhile, the circulations adjacent to the homogeneous and heterogeneous surfaces gradually lose their strength and shrink in size. At $t = 7.5$, no electrokinetic body force exists within the double layer, but the streamwise flow velocity approaches its positive maximum value. Hence, the fluid velocity in the entire micro-channel becomes positive, and the streamline contour assumes a stratified form. During the second half of the cycle, i.e., from $t = 7.5$ to 8, the variation of the applied AC electric field intensity is the mirror image of the variation described from $t = 7$ to 7.5, and accordingly, the bulk flow velocity in the micro-

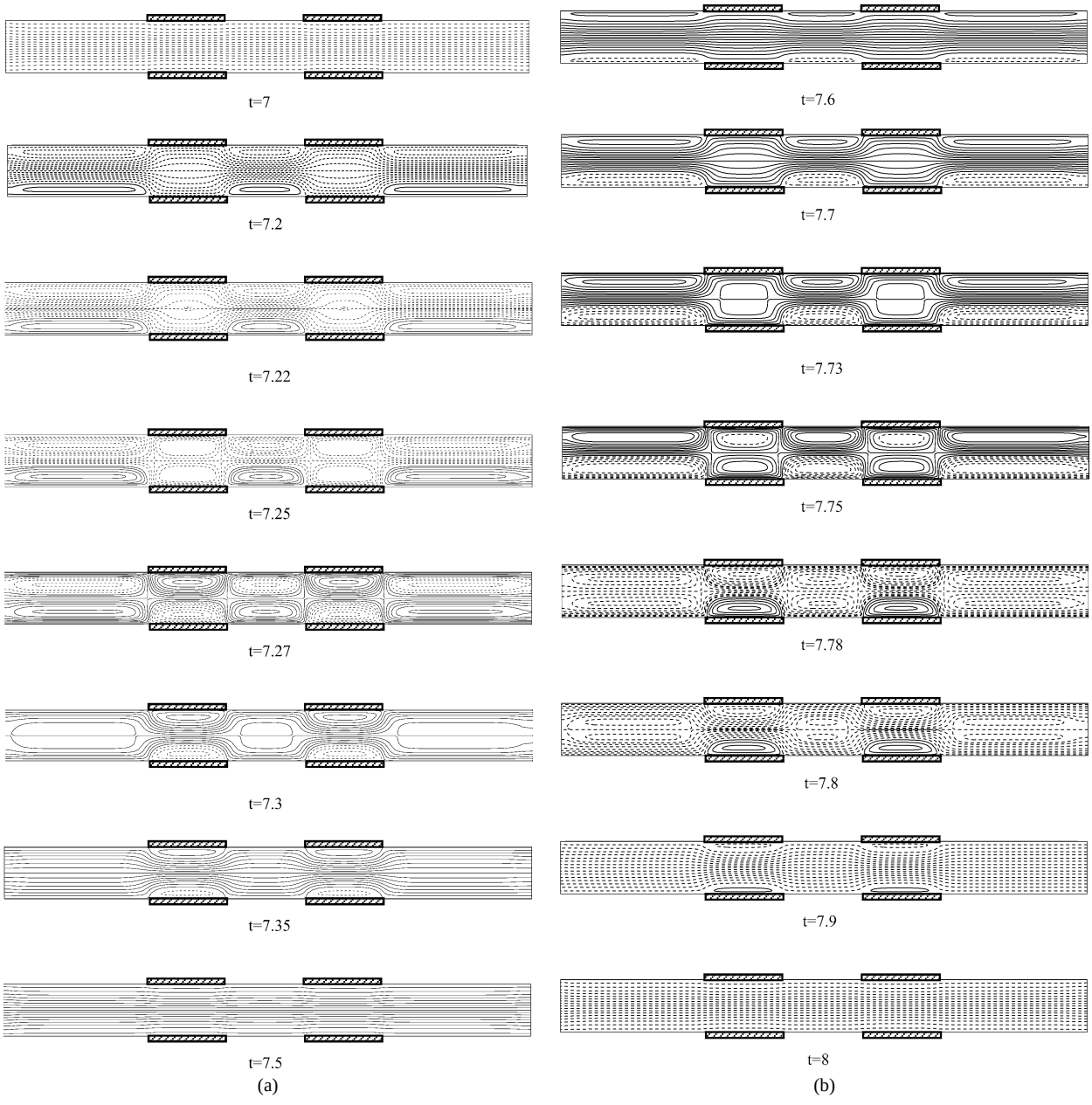

Fig. 7. (a) Flow evolutions in micro-channel with two symmetrically positioned heterogeneous patches (Type III) from $t = 7$ to 7.5. (b) Flow evolutions in micro-channel with two symmetrically positioned heterogeneous patches (Type III) from $t = 7.5$ to 8.

channel reverses from a positive maximum value to a negative value. This causes the fluid flows within the double layer to change their respective directions of travel, i.e., the fluid near the homogeneous surface is driven in the negative X-direction, while the fluid near the heterogeneous surface is driven in the positive X-direction. New circulations, rotating in the opposite direction to those in the previous half-cycle, are formed adjacent to the homogeneous surfaces under the influence of the negative intensity of the applied electric field and the positive bulk flow velocity, as shown in Fig. 7b. The structures of the newborn circulations gradually become more coherent over time, and grow in size and strength. Essentially, the evolution of the flow conditions during the cycle from $t = 7.5$ to 8 follows the same process as that described for $t = 7$–7.5, but the directions of the circulations and bulk flow are the exact reverse of those observed during the period $t = 7$–7.5. At time $t = 8$, the intensity of the applied electric field changes suddenly from negative to positive, and the streamwise velocity of the micro-channel approaches its negative minimum value. The flow conditions at this time are identical to those observed at $t = 7$. The evolution of the flow conditions during the cycle from $t = 8$ to 9 follows the same process as that described for $t = 7$–8. In general, it can be speculated that the size and intensity of the circulations are determined by the phase shift between the applied electric field and the bulk flow velocity. When the phase of the bulk flow velocity lags behind that of the applied electric field by approximately π degrees, the intensity of the electric field and the bulk flow velocity reach their maxi-

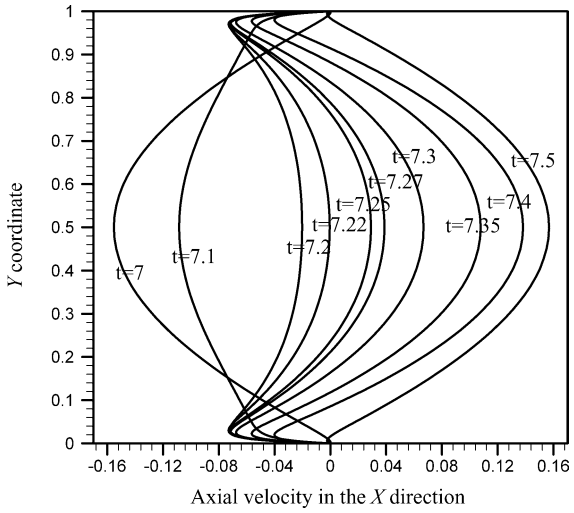

Fig. 8. Axial velocity distributions along Y-axis at $X = 105$ μm during period $t = 7$–7.5 in micro-channel with two symmetrically positioned heterogeneous patches.

mum values, although in opposite directions, at the same time, and the inertia force of the bulk flow suppresses the growth of the induced circulations.

Fig. 8 indicates the axial velocity distributions along the Y-axis at $X = 105$ μm during a half period $t = 7$–7.5. At $X = 105$ μm, the surfaces of the upper and lower walls are heterogeneous. From $t = 7$ to 7.5, the applied sinusoidal electric field has a positive intensity. In Fig. 8, as time elapses, the fluid within the double layer is gradually driven to move in the positive axial direction. Through the effects of momentum diffusion and inertia force, the bulk flow is gradually dragged into motion from a negative velocity to a positive velocity in the axial direction. The evolution of the velocity distribution along the Y-axis during the period $t = 7.5$–8 follows a similar process to that described above for $t = 7$–7.5. However, the direction of the fluid flow in the micro-channel is reversed.

5. Conclusion

This paper has investigated two-dimensional, time-dependent electroosmotic flows driven by a sinusoidal AC electric field of amplitude 450 V/cm and frequency 1000 Hz in micro-channels with a homogeneous surface or with various distributions of surface heterogeneities. The time-dependent flow fields through the micro-channels were simulated using the backwards-Euler time stepping numerical method. By solving the Laplace, Poisson, and vorticity transport equations simultaneously, the electric field, the double layer distribution, and the flow field were determined.

It has been shown that different distributions of the surface heterogeneities have dramatically different effects on the flow field phenomena. In the case of the micro-channel with a series of symmetrically distributed heterogeneous patches on the upper and lower walls, the application of a sinusoidal electric field results in the formation of a sequence of local circulations with alternating rotational directions along the axial direction of the micro-channel. These circulations settle symmetrically in the upper and lower regions of the micro-channel adjacent to the homogeneous and heterogeneous surfaces and constrain the flow to a converged narrow stream through the middle of the channel. Meanwhile, for the micro-channel with a series of offset heterogeneous patches on the upper and lower walls, the applied sinusoidal electric field prompts the formation of a sequence of regional circulations adjacent to the homogeneous or heterogeneous surfaces and induces tortuous streamlines within the bulk flow. The size and strength of the regional circulations grow and decay periodically in phase with the intensity of the applied electric field. The rotational directions of the induced circulations and the positions of the circulations are determined by the streamwise velocity of the bulk flow and the direction of the applied electric field. Under the influence of the positive applied electric field, the induced circulations settle adjacent to the homogeneous surfaces when the bulk flow moves in the negative axial direction. Conversely, the circulations settle adjacent to the heterogeneous surfaces when the bulk flow moves in the positive axial direction. Under the negative applied electric field, the induced circulations settle adjacent to the homogeneous surfaces when the bulk flow moves in the positive axial direction, and settle adjacent to the heterogeneous surfaces when the bulk flow moves in the negative axial direction. The size and intensity of the circulations are governed by the zeta potentials of the homogeneous and heterogeneous surfaces, the intensity of the applied electric field, the axial velocity of the bulk flow in the micro-channel, and the phase shift between the applied electric field and the bulk flow velocity.

Acknowledgment

The current author wishes to acknowledge the financial support provided to this study by the National Science Council under Grant No. NSC 93-2212-E-269-001.

References

[1] N.A. Patankar, H.H. Hu, Anal. Chem. 70 (1998) 1870–1881.
[2] R.J. Yang, L.M. Fu, Y.C. Lin, J. Colloid Interface Sci. 239 (2001) 98–105.
[3] F. Bianchi, R. Ferrigno, H.H. Girault, Anal. Chem. 72 (2000) 1987–1993.
[4] S. Arulanandam, D. Li, Colloids Surf. A 161 (2002) 89–102.
[5] O. Soderman, B. Jonsson, J. Chem. Phys. 105 (1996) 10300–10311.
[6] G.J. Santiago, Anal. Chem. 73 (2001) 2353–2365.
[7] M.H. Oddy, J.G. Santiago, J.C. Mikkelsen, Anal. Chem. 73 (2001) 5822–5832.
[8] P. Dutta, Beskok, Anal. Chem. 73 (2001) 5097–5102.
[9] V. Studer, A. Pepin, Y. Chen, A. Ajdari, Microelectron. Eng. 61–62 (2002) 915–920.
[10] N.G. Green, A. Ramos, A. Gonzalez, H. Morgan, A. Castellanos, Phys. Rev. E 61 (2000) 4011–4018.
[11] W.J. Luo, J. Colloid Interface Sci. 278 (2004) 497–507.
[12] W.J. Luo, Y.J. Pan, R.J. Yang, J. Micromech. Microeng. 15 (2005) 463–473.
[13] A. Ajdari, Phys. Rev. Lett. 75 (1995) 755.
[14] S. Qian, H.A. Bau, Anal. Chem. 74 (2002) 3616.
[15] A.D. Strook, M. Weck, D.T. Chiu, W.T.S. Huck, P.J.A. Kenis, R.F. Ismagilov, G.M. Whitesides, Phys. Rev. Lett. 84 (2000) 3314.
[16] D. Ericson, D. Li, Langmuir 18 (2002) 1883.
[17] E. Biddiss, D. Erickson, D. Li, Anal. Chem. 76 (2004) 3208.
[18] C.C. Chang, R.J. Yang, J. Micromech. Microeng. 14 (2004) 550–558.

[19] J.S.H. Lee, C.L. Ren, D. Li, Anal. Chim. Acta 530 (2005) 273.
[20] R.J. Hunter, Zeta Potential in Colloid Science: Principals and Applications, Academic Press, New York, 1981.
[21] C. Yang, D. Li, Colloids Surf. A 143 (1998) 339–353.
[22] R.J. Yang, W.J. Luo, Theoret. Comput. Fluid Dynamics 16 (2002) 115–131.